Heat Transfer in Rotating Rectangular Cooling Channels (AR=4) With Dimples

Todd S. Griffith

Luai Al-Hadhrami

Je-Chin Han

Turbine Heat Transfer Laboratory,
Department of Mechanical Engineering,
Texas A&M University,
College Station, TX 77843-3123

As the world of research seeks ways of improving the efficiency of turbomachinery, attention has recently focused on a relatively new type of internal cooling channel geometry, the dimple. Preliminary investigations have shown that the dimple enhances heat transfer with minimal pressure loss. An investigation into determining the effect of rotation on heat transfer in a rectangular channel (aspect ratio*=4:1) with dimples is detailed in this paper. The range of flow parameters includes Reynolds number (Re=5000–40000), rotation number (Ro=0.04–0.3) and inlet coolant-to-wall density ratio ($\Delta\rho/\rho$ =0.122). Two different surface configurations are explored, including a smooth duct and dimpled duct with dimple depth-to-print diameter (δ/D_p) ratio of 0.3. A dimple surface density of 10.9 dimples/in^2 was used for each of the principal surfaces (leading and trailing) with a total of 131 equally spaced hemispherical dimples per surface; the side surfaces are smooth. Two channel orientations of $\beta=90$ and 135 deg with respect to the plane of rotation are explored to determine channel orientation effect. Results show a definite channel orientation effect, with the trailing-edge channel enhancing heat transfer more than the orthogonal channel. Also, the dimpled channel behaves somewhat like a 45 deg angled rib channel, but with less spanwise variations in heat transfer.*
[DOI: 10.1115/1.1571850]

Keywords: Heat Transfer, Dimple, Channel, Rotating

Introduction

Extensive research efforts have recently focused on methods for reducing the consumption of non-renewable energy resources. The turbomachinery industry is one industry committed to improving the efficiency of its equipment. Gas turbines are used for a wide variety of applications including power generation, gas compression, and jet propulsion. The efficiency of a turbine can be increased by increasing the combustion temperature or decreasing the amount of compressor dilution air used to cool the extremely hot gas exiting the combustor. This poses a major problem in the hastened degradation of temperature sensitive components of the turbine, principally the turbine blades and vanes. To counter the high turbine inlet temperatures (1600–1800 K), the physics of turbulent heat transfer under rotation are investigated in a cooling model. Turbine blades incorporate internal cooling passages to extract the thermal energy absorbed from the hot combustion gases. This prolongs the life of the blade as well as allowing for increased combustion temperatures, which ultimately increases performance of the turbine.

A small amount of pressurized air is extracted from the compressor and injected into the turbine blades via the cooling air bypass. This relatively low enthalpy gas is forced through the internal cooling passages of the turbine blades, convectively extracting heat from the internal walls. For further thermal protection of the blade, a portion of the internal cooling air is ejected through tiny holes in the walls and tip of the blade, creating a cool film thermal boundary.

When considering the effects of rotation, certain flow phenomena are exhibited that are not observable in the stationary reference frame. Forces are generated under rotation, principally the Coriolis and buoyancy forces. These forces generate a secondary flow in the plane orthogonal to the mean flow direction. For radial outward flow, the Coriolis and buoyancy forces combine to shift the velocity profile toward the trailing surface. The coolant flow migrates along with the heat transfer augmentation toward the trailing surface. This rotationally induced migration of the cooler core flow results in the advantageous enhancement of heat transfer at the trailing surface, but it is typically balanced by the disadvantageous reduction in heat transfer from the leading surface. As with most temperature sensitive components, thermal failure in an isolated region is oftentimes just as problematic as failure of the entire component. This is why it is important to analyze the heat transfer phenomenon segment by segment along the length of the blade.

The aspect ratio of the channel also has a profound impact on the effect of rotation. Moving from the midchord to the trailing edge of the blade, the channels must become more rectangular as the blade becomes thinner. The orientation of a 4:1 aspect ratio cooling channel in a gas turbine blade is shown in Fig. 1. This thinning of the channel changes the effective secondary flow pattern from that of a square duct. For this reason, one cannot simply apply the knowledge of the rotationally induced flow patterns in a square channel to that of a rectangular channel. Therefore, an investigation of the rectangular channel is necessary to further understand the heat transfer characteristics of the internal cooling channels in a gas turbine blade.

To promote heat transfer in the internal cooling passages, various types of turbulators are used to trip the boundary layer. Ribs or ''trip-strips'' and pin-fins have been commonly used in gas turbines over the past decade. The dimple is a relatively new approach, investigated first by Schukin et al. [1]. When combining the effects of tripping the boundary layer (using ribs, pins, or dimples) and rotational forces (Coriolis and buoyancy), entirely different turbulence and flow phenomenon are achieved. Combining into this equation the various shapes and sizes of internal cooling channels, it is clear that there is no one single solution that can be applied universally in the field of turbine heat transfer. For this reason, an experimental investigation into each combination of the previously mentioned parameters is necessary.

Contributed by the International Gas Turbine Institute and presented at the International Gas Turbine and Aeroengine Congress and Exhibition, Amsterdam, The Netherlands, June 3–6, 2002. Manuscript received by the IGTI January 18, 2002. Paper No. 2002-GT-30220. Review Chair: E. Benvenuti.

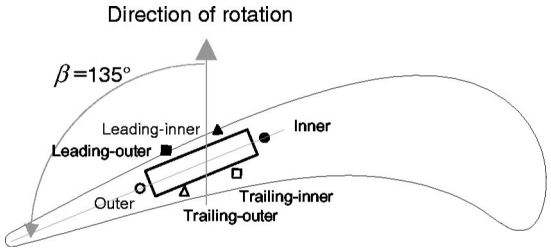

Fig. 1 Sketch illustrating orientation of a 4:1 aspect ratio channel in a gas turbine blade

Numerous studies on turbulent flow and heat transfer in the cooling channels of a gas turbine blade have been performed in the past. Han and Park [2] published experimental investigations of the heat transfer phenomenon in a stationary rib roughened rectangular channel. Wagner et al. [3,4] conducted detailed experimental investigation to determine the effects of rotation, or more specifically the effects of Coriolis and buoyancy forces on the regionally averaged heat transfer distribution of a serpentine square channel with smooth walls. This study determined that in the first pass, the effect of rotation created a thinner boundary layer on the trailing surface and a thicker boundary layer on the leading surface.

Parsons et al. [5] studied the effects of channel orientation and wall heating condition on the regionally averaged heat transfer coefficients in a rotating two-pass square channel with ribbed walls. They discovered that the heat transfer enhancement for the constant wall heat flux boundary condition was more pronounced if the duct is twisted 45 deg to the plane of rotation when compared to a channel oriented orthogonal to the plane of rotation. Johnson et al. [6] determined that the model orientation with respect to the rotation plane greatly affected the heat transfer distribution.

Dutta and Han [7] investigated the regionally averaged heat transfer coefficients in a rotating two-pass square channel with three different model orientations. They found that the orientation of the channel with respect to the plane of rotation affected the heat transfer distribution. More specifically, they determined that orienting the channel at an angle with respect to the plane of rotation reduced the effect of rotation when compared to the orthogonal channel orientation.

Until recently, most of the experimental studies have explored only square ducts. However, it is quite common to find rectangular cooling passages, particularly toward the trailing edge of a gas turbine blade. Since the profile of a turbine blade is curved, the exclusive use of square channels is not practical. Past research focused mainly on the square channel; therefore, published data for a rectangular cooling channel is rare.

Willett and Bergles [8] performed a detailed investigation of the heat transfer in a narrow, 10:1 smooth rectangular channel oriented at 60 deg to the *r-z* plane. Most of their focus dealt with exploring the contribution of buoyancy forces under rotation. They found that the duct orientation induced a significant heat transfer gradient in the spanwise direction. It was also found that the normalized Nusselt number at the far-aft-end of the trailing side (or the trailing-outer equivalent in this paper) is a strong function of rotation number and buoyancy number.

Griffith et al. [9] studied the effects of rotation on a AR=4:1 rectangular channel with $\beta=90$ and 135 deg. They determined that the rib induced secondary flow dominated the rotation-induced vortices, particularly at lower rotation numbers. They also found that significant spanwise heat transfer gradients exist for both channel orientations.

Dimpled channel literature has surface quite recently. Ekkad et al. [10] used cylindrical dimples with several different depths to simulate the TBC spallation for flow over a flat plate. The paper

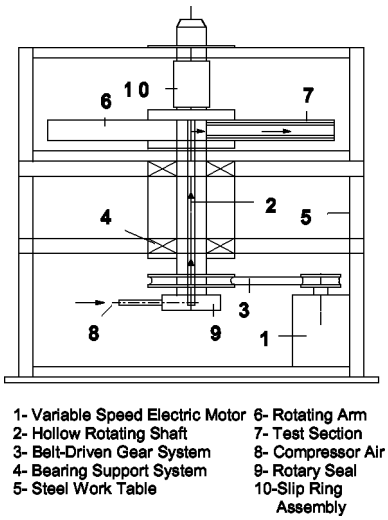

Fig. 2 Schematic of experimental rotating test rig

also used other geometries such as square, rectangular, diamond, and elliptic shape of dimples. Azad et al. [11] Investigated a channel with cylindrical dimples on the target walls of impingement cooling, instead of the concave (hemispherical) dimples as in the current study.

Chyu et al. [12] investigated hemispheric and teardrop shaped concavities in a stationary channel using a liquid crystal technique. They found that the overall performance was nearly equal for the geometries, showing enhancement of approximately 2.5 times that of a smooth duct for the stationary case. Moon et al. [13] analyzed a stationary dimpled channel using a liquid crystal technique. They found that the heat transfer enhancement occurs mostly outside of dimples. They also found that the enhancement is reduced in the upstream portion of dimple and the enhancement is increased in the downstream portion (rim) of dimple. In addition, they determined that enhancement not a function of Reynolds number, and is typically constant at around 2.1. Mahmood et al. [14] investigated a stationary dimpled channel using infrared thermography and smoke-stream flow visualization. They found that a large upwash region occurs in the center of the dimple, and pairs of vortices are shed at the dimple diagonals. They also determined that the enhancement principally occurs on the plateau (or flat) surface. Zhou et al. [15] used the concave dimples on the leading and trailing surfaces of a rotating square channel.

For a more comprehensive compilation of turbine heat transfer research, please see the book by Han et al. [16] and review paper by Han and Dutta [17].

Considering that the effect of rotation has shown to significantly influence the heat transfer enhancement of a cooling channel, it is of interest to explore the rotational effects on the heat transfer in a dimpled channel. The following questions arise:

1. How does the spanwise heat transfer distribution vary within a dimpled, rotating, rectangular channel?
2. How does the dimpled channel compare to a smooth and ribbed channel?
3. What is the effect of the channel orientation with respect to the plane of rotation?
4. How do rotational forces quantitatively influence the heat transfer enhancement in a dimpled rectangular channel?

Answers to these questions are pursued in this paper.

Experimental Facility

The experimental test rig previously used by Dutta and Han [7] is utilized in this investigation (see Fig. 2). A variable frequency

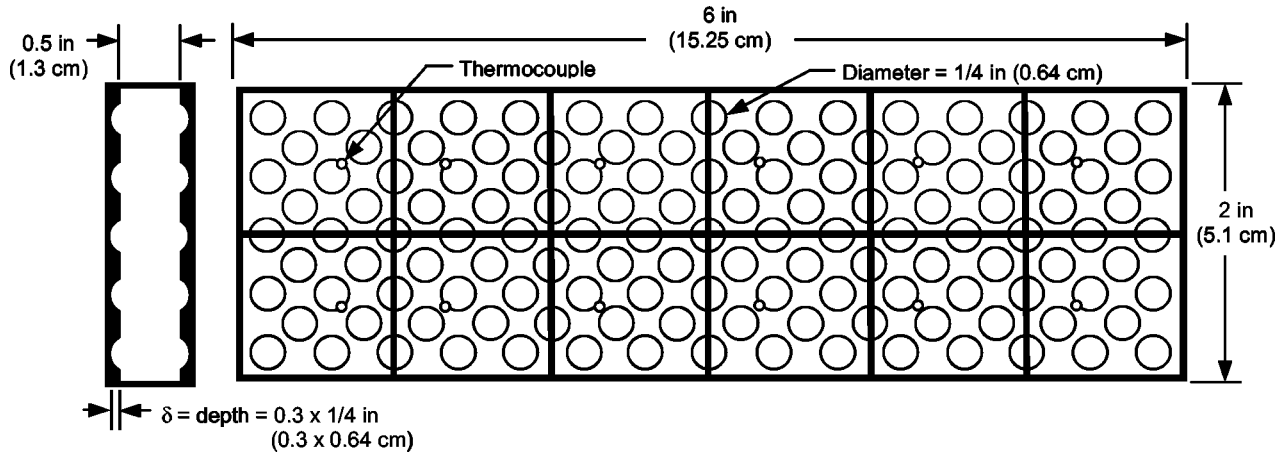

Fig. 3 Schematic of 4:1 dimpled test

motor is connected via a gear-and-belt mesh to a hollow, rotating shaft. This shaft runs from the base of the test rig to the work platform and is attached orthogonal to the hollow, rotating arm. The test section is inserted inside the hollow rotating arm, which rotates in a plane orthogonal to the rotating shaft. A hand held optical tachometer is used to determine the rotational velocity of the arm. Thermocouple and heater wires are connected to a 100-channel slip-ring assembly mounted to the rotating shaft. The output of the thermocouples is transferred to a data logger. Fuse-protected power input to the heaters from the variac transformers is also transmitted through the slip ring assembly. Cooling air is pumped from a steady flow compressor, through an ASME orifice flow meter, then through the hollow rotating shaft, turning 90 deg and passing into the rotating arm, then through the test section and is finally expelled into the atmosphere.

The test section is a 0.5-in. by 2-in. by 6-in.-long ($1.27\times5.08\times15.24$ cm) one-pass rectangular channel of aspect ratio 4:1 with a hydraulic diameter of D=0.8 in. Preceding the test section is an 8-in.-long (20.3-cm) smooth, unheated entrance length (same rectangular cross-section), sufficiently long enough to provide hydrodynamically fully developed flow at the entrance to the test section. The ratio of mean rotating radius to hydraulic diameter is $R/D=33$. The direction of airflow is radially outward from the axis of rotation. Two rows of copper plates are installed on both the leading and trailing surface to provide a grid for analysis of the spanwise variation in the regionally averaged heat transfer coefficient.

Figure 3 shows a detailed top view of the test section. The test section is divided into six cross-sections, each with six copper plates: two for the leading, two for the trailing, one for the outer and one for the inner surface. Moving along the direction of the flow (radially outward), there are six streamwise segments for a total of 36 copper plates in the entire test section. The channel length-to-hydraulic diameter ratio (L/D) is 7.5 with a ratio of 1.25 for each of the six cross section segments. Each plate is separated by a 0.0626-in. (0.159-cm) thin strip of nylon to prevent heat conduction between plates. This is important since the objective is to study the spatial distribution of heat transfer.

The copper plates are mounted in a nylon substrate, which comprises the bulk of the test section. Prefabricated flexible heaters are installed beneath the leading and trailing surfaces, two to each surface. The outer and inner walls (or side walls) are each heated by a wire-wound resistance heater, which is also installed beneath the copper plates. All heaters supply steady, uniform heat flux to the copper plates. Sufficient power is supplied in order to maintain a maximum wall temperature of nearly 340 K for the corresponding section. This corresponds to an inlet coolant-to-wall density (temperature) ratio $(\Delta\rho/\rho)_i$ of 0.122 for every test. Thermal conducting paste is applied between the heater and copper plates to promote heat transfer from the heater to the plate. Each 1/8-in. (0.318-cm) thick plate has a 1/16-in. (0.159-cm) deep blind hole drilled in the backside in which a copper-constantan thermocouple is installed 1/16 in. (0.159 cm) from the plate surface with thermal conducting glue.

Two different surface configurations (smooth and dimpled $\delta/D_p=0.3$) are studied as well as two different channel orientations with respect to the direction of rotation ($\beta=90$ and 135 deg). For the dimpled experiments, only the leading and trailing surfaces are dimpled with the side surfaces kept smooth. The dimples are machined using hemispherical end-mills. The experiments were conducted for Reynolds numbers of 5000, 10000, 20000, and 40000. The test section rotates at a constant speed of 550 rpm resulting in a range of rotation number (R_o) from approximately 0.04–0.3.

Data Reduction

This investigation focuses on detailing the regionally averaged heat transfer coefficient at various locations within the internal cooling channel. This heat transfer coefficient is determined by the net heat flux from the heated plate to the cooling air, the regionally averaged temperature of the plate, and the local bulk mean air temperature by the following:

$$h=q''_{\text{net}}/(T_w-T_{b,x}) \tag{1}$$

The net heat flux is calculated using the measured voltage and current supplied to the heater multiplied by the area fraction exposed to the respective plate minus the previously determined amount of heat losses due to external conduction, convection, and radiation energy escaping from the test section. This heat loss calibration is performed for both stationary and rotation experiments with a piece of insulation inserted inside the test section to inhibit natural convection. For this calibration, by knowing the amount of power supplied to the heater and measuring the temperature of the plate, it is possible to determine how much the heat is being lost into the environment using the conservation of energy principle. Equation 1 is used throughout the experiment, neglecting the change of area effect with the addition of dimples. That is, the heat transfer coefficient is calculated based on the projected area, neglecting the 19.3% increase in area due to the addition of dimples.

The regionally averaged wall temperature (T_w) is measured directly by the thermocouple installed in the back of each plate. The local bulk mean air temperature ($T_{b,x}$) is determined by a linear interpolation between the measured bulk air inlet and the average of two outlet temperatures (each installed at the midpoint

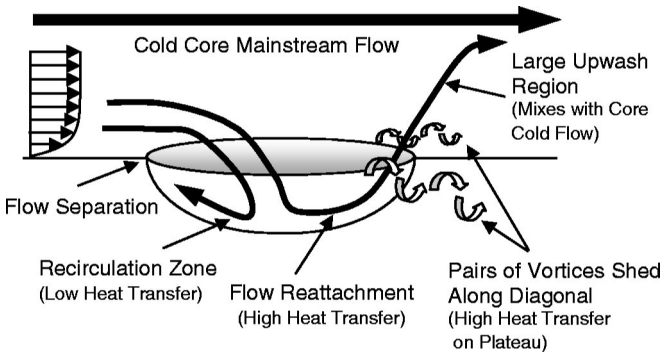

Fig. 4 Dimple induced secondary flow (conceptualization)

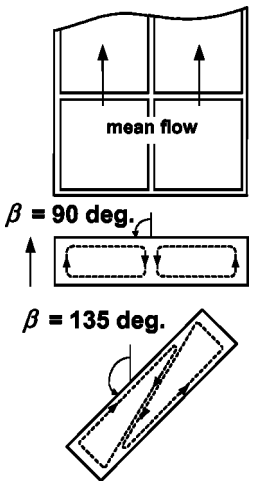

Fig. 5 Rotation-induced (Coriolis force) vortices in rectangular channel

of the two spanwise sections) due to the applicable constant heat flux assumption. Another method used to check the interpolation values is by performing an energy balance. It is reassuring to note that performing an energy balance to calculate the expected outlet temperature resulted in a close match to that of the average measured exit temperature value, typically to within 5%. Therefore the linear interpolation method is validated and is the method used in the calculation of the results presented in this paper. The energy balance equation is

$$T_{b,i} = T_{in} + \sum_i (q - q_{\text{loss}})/\dot{m}c_p, \quad i = 1,2 \ldots 6 \tag{2}$$

To provide a common reference for each analysis, a correlation is used comparing the Nusselt number for the specific duct case to that of fully developed flow through a smooth stationary pipe at the same Reynolds number. For this investigation, the Dittus-Boelter correlation for heating ($T_w > T_{bx}$) is used [18]

$$\frac{\text{Nu}}{\text{Nu}_o} = \frac{hD}{k_{\text{air}}} \frac{1}{(0.023\,\text{Re}^{0.8}\,\text{Pr}^{0.4})} \tag{3}$$

All air properties are taken based on the mean bulk air temperature with the Prandtl number (Pr) for air as 0.71.

Overall uncertainty for the regionally averaged heat transfer coefficient is predominantly dependent upon the difference between the wall temperature and the bulk air temperature, the net heat flux input and the ability to maintain a steady mass flow rate. As with most experiments, the uncertainty for this investigation decreases with the increasing magnitude of input parameters. For higher Reynolds numbers, the uncertainty has been determined to be nearly 7%. However, for lower Reynolds number (Re $=5000$), the uncertainty could be as much as 20%. The uncertainty analysis was performed using the Kline and McClintock [19] uncertainty analysis procedure.

Results And Discussion

The surface labeling scheme, seen in Fig. 1, will be used throughout this paper. The inner and outer surface side walls are named according to their location in the turbine blade. That is, the inner surface is closer to the mid-chord position of the blade (a relatively internal position), and the outer surface is closer to the trailing edge of the blade, and thus is closer to an external surface of the blade. The leading and trailing surfaces of the blade follow the conventional definitions of these surfaces, however each surface is subdivided into two surfaces in order to investigate the span-wise distribution of heat transfer along the major surfaces (leading and trailing). Therefore we have a total of six surfaces: leading-outer, leading-inner, trailing-outer, trailing-inner, outer, and inner. A brief discussion on the secondary flow pattern induced by a dimple is presented in the forthcoming.

Secondary Flow Behavior. Figure 4 shows a conceptualization of the secondary flow patterns over a dimpled surface. As the flow approaches the upstream portion of the dimple, flow separation occurs, and a recirculation zone appears in the upstream portion of the dimple resulting in mitigation of the heat transfer. As the flow reattaches at the downstream half of the dimple, an increase in the heat transfer enhancement occurs. Continuing in the streamwise direction, it has been shown that a large upwash region is produced by the dimple. This upward directed flow mixes to some degree with the cold core mainstream flow. Finally, pairs of vortices are shed along the dimple diagonals, enhancing the heat transfer on the flat portion of the surface. Considering the dimple induced secondary flows and superimposing the rotation induced secondary flow upon it, it is apparent that there is no primarily constructive combination of the two, as was shown in the case of a 45 deg angled-rib rotating channel investigated by Griffith et al. [9]. This complex combination of the dimple induced vortices in various directions with the rotation induced secondary flow does not generate any vision of a primary coherent flow structure, however the heat transfer enhancement is still increased at the trailing surface due to the thinning of the boundary layer under rotation.

Figure 5 shows a conceptualization of the secondary flow induced by rotating a smooth, rectangular channel. The Coriolis force induces two counter rotating vortices, which serve to push the colder fluid closer to the trailing surface. When the channel is twisted such that $\beta = 135$ deg, the linear distance of the Coriolis force main vector increases from a relatively small distance (as in the case of $\beta = 90$ deg to a much longer distance. The Coriolis vector now traverses the diagonal from the leading most corner to the trailing most corner of the twisted channel. This shifting of the rotation induced vortices serves to mix the flow more effectively.

Smooth Channel Results. Figures 6–8 contain the smooth duct data for three different channel configurations: stationary, rotation with $\beta = 90$ deg and rotation with $\beta = 135$ deg. Each case is subdivided into four experiments: (*a*) Re $=5000$, (*b*) Re $=10000$, (*c*) Re $=20000$, and (*d*) Re $=40000$. The corresponding rotation numbers for these cases are 0.305, 0.151, 0.075 and 0.038 respectively. Figure 6 contains data for the stationary cases. The initial decrease in the normalized Nusselt number plots is attributable to the entrance effect in thermally developing flow. The plots all approach a horizontal asymptote as the flow approached the thermally fully developed state.

Figure 7 shows the results for the rotation cases where the duct is oriented at $\beta = 90$ deg, that is, orthogonal to the plane of rotation. As was expected, the trailing surfaces exhibit higher heat

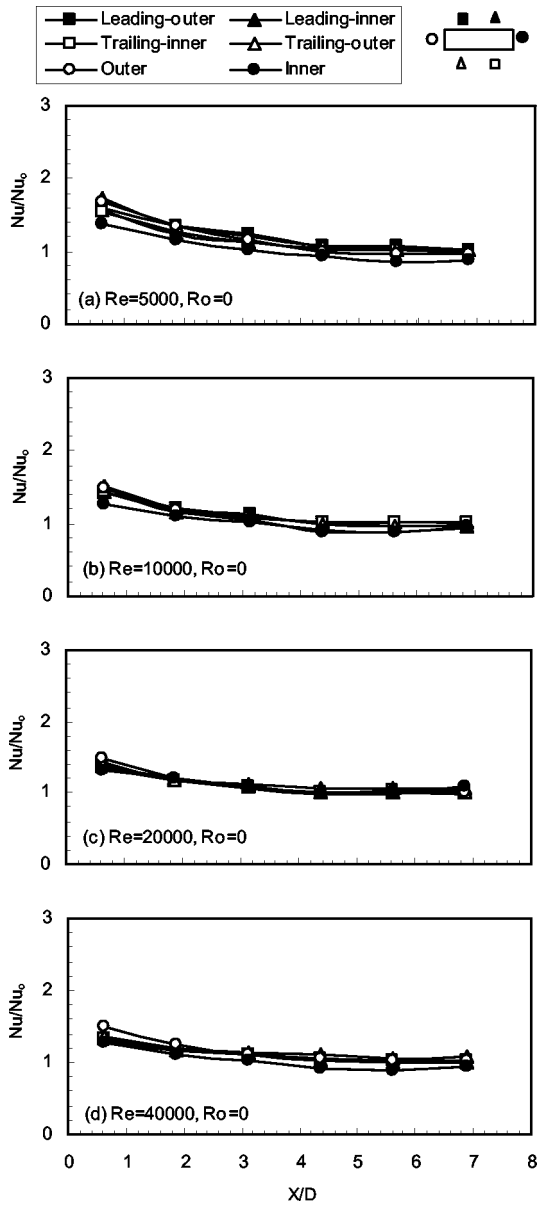

Fig. 6 Nusselt number ratio for stationary smooth case

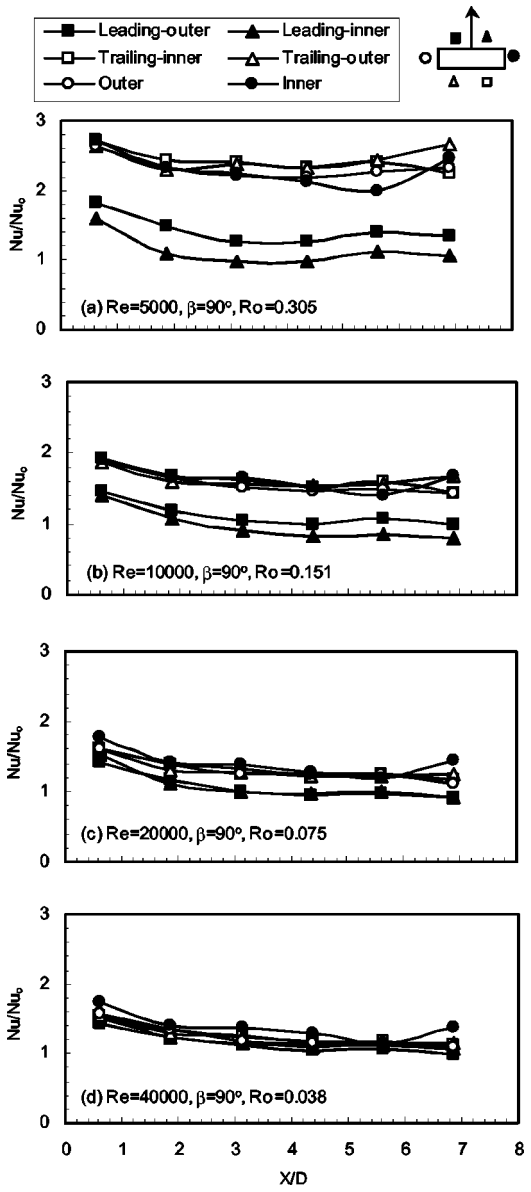

Fig. 7 Nusselt number ratio for rotation smooth case with β=90 deg

transfer enhancement than the leading surfaces due to the migration of the colder core fluid toward the trailing surface caused by the Coriolis rotational forces. At a duct angle of β=90 deg, the channel can be assumed to hold symmetry about the plane of rotation. This means that both of the leading surfaces (leading-outer and leading-inner) should have identical Nu plots, the trailing surfaces should exhibit identical behavior, and the two side surfaces should be equal. This is validated relatively well as seen in the figures, with a slight bias between the two trailing surfaces. An increase in the Reynolds number tends to suppress the effect of rotation. All six surfaces show very little streamwise variation in the Nu number plots. Both of the side surfaces (inner and outer) have a heat transfer enhancement nearly equal to the value of the two trailing surfaces.

Figure 8 presents the results of the smooth rotation case with the channel oriented at β=135 deg with respect to the plane of rotation. Figure 8*a* shows that at a low Reynolds number (high rotation number), there are distinguishable differences in the heat transfer trends among the various surfaces. It can be seen that the trailing-outer and outer surfaces exhibit the highest heat transfer enhancement of all of the surfaces in the duct. This is attributed to the fact that these two surfaces are the primary recipients of the shifting of the cooler core flow under rotation. This phenomenon is illustrated in Fig. 5 of the preceding section. After the flow impinges on the trailing-outer and outer surfaces, it passes along the leading and trailing surfaces to the inner surface, where the heat transfer coefficient is the lowest, and the secondary flow slows down dramatically. Then the flow cycles again, passing from the leading most corner diagonally across the channel toward the trailing most corner. At a high rotation number, the inner surface heat transfer follows a trend quite similar to the stationary cases. It appears that this inner surface is barely affected by rotation. Both of the trailing surfaces have higher heat transfer coefficients than the leading surfaces. A new and interesting finding is the substantial difference in the heat transfer coefficient between the two trailing surfaces. Furthermore, this span-wise difference does not come into effect until nearly half-way through the channel for high rotation numbers (R_o=0.305). It is also shown that the leading surface heat transfer increased when compared to the orthogonal channel. The overall increase in heat transfer from

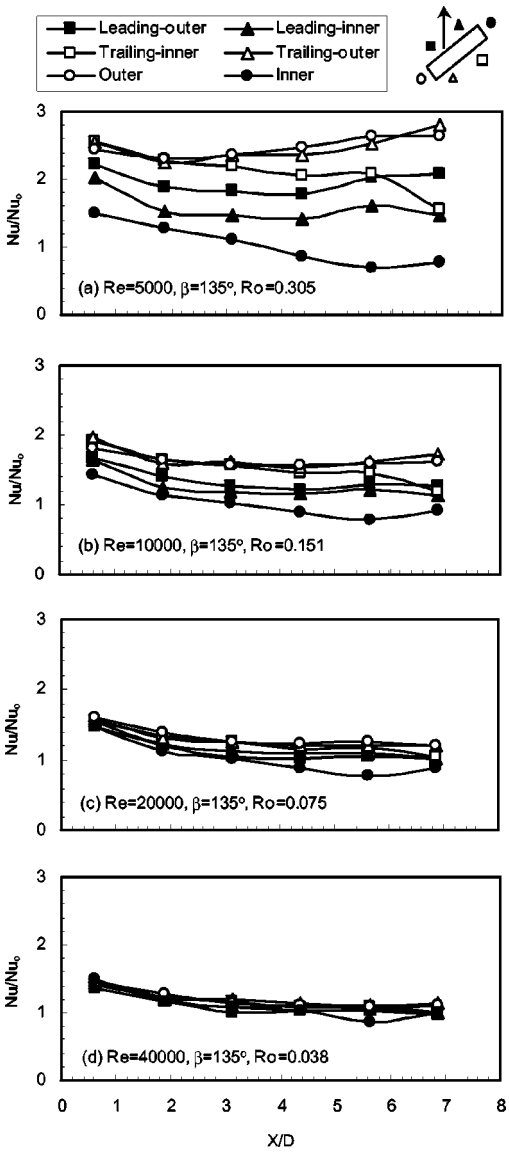

Fig. 8 Nusselt number ratio for rotation smooth case with β=135 deg

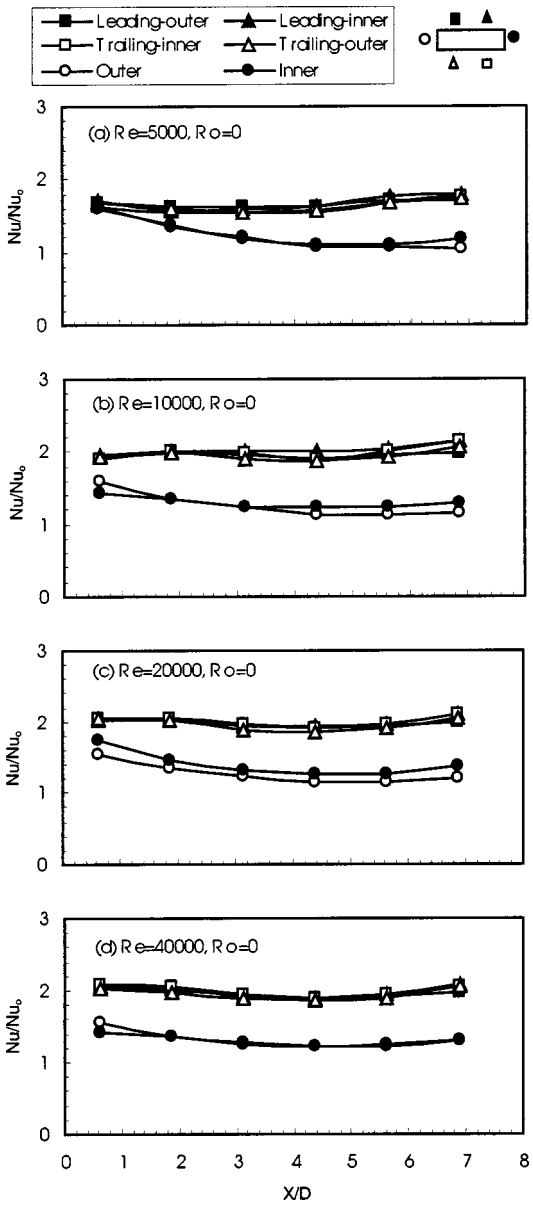

Fig. 9 Nusselt number ratio for stationary dimpled case

nearly all surfaces can be attributed to the fact that twisting the channel greatly increased the linear distance along which the main Coriolis force is directed (from leading most to trailing most corner) and provides an overall better mixing than the β=90 deg case. In the β=90 deg case, the principal Coriolis vector in the core region of the flow acts across only a short distance (the short width of the channel) and does not serve to mix the flow as well as the twisted channel.

One evident contrast of the results of the β=135 deg case (Fig. 8) compared to the β=90 deg (Fig. 7) case is apparent in the side surfaces. For the twisted channel, the trend of the outer surface increases while the inner surface trend decreases with X/D. Furthermore, the inner surface decreases in a similar way as seen in the stationary case. The outer surface, which trails after the inner surface, experiences a heat transfer enhancement of as much as three times that of the inner surface for the β=135 deg case. This is due to the shift of the primary Coriolis induced flow vector from the center of the trailing surface in the β=90 deg case to the trailing most corner in the β=135 deg case. This trailing most corner is adjacent to the outer surface, and therefore the outer surface benefits greatly in heat transfer enhancement due to the twisting of the duct. This is desirable since the outer surface of the β=135 deg case is closer to the trailing edge of the turbine blade, and thus is likely to experience a higher external heat flux than the inner surface. The inner surface interfaces with the side surface of the adjacent cooling passage, and therefore is less likely to be considered a critical surface.

Dimpled Channel Results. The data plots for the dimpled channel cases are presented in Figures 9–11. Figure 9 shows the stationary dimpled channel results. An enhancement of approximately 2.0 is produced by the dimpled surface. This is in close agreement with the results of Moon et al. [10]. The smooth side surfaces (inner and outer) appear to only benefit marginally from the mixing induced by the dimpled surfaces. It is shown that for Reynolds numbers 10000, 20000, and 40000, there appears to be almost no dependence upon Reynolds number. This observation was also made in the past by Moon et al. [10]. However, when the data for Re=5000 is considered, we see the emergence of Reynolds number dependence, with the enhancement decreasing with decreasing Reynolds number, but only at the lowest Re value.

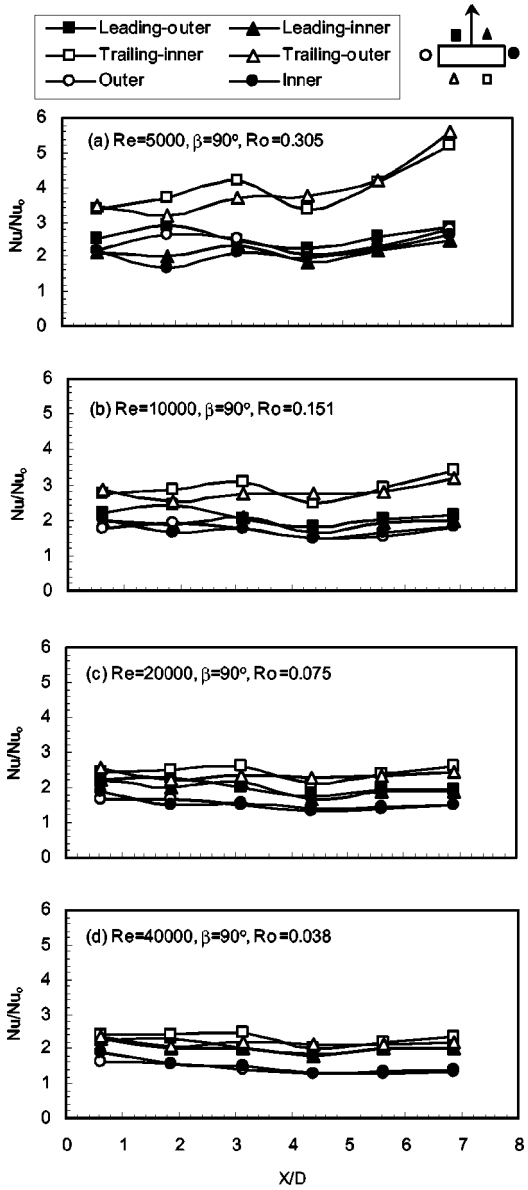

Fig. 10 Nusselt number ratio for rotation dimpled case with β=90 deg

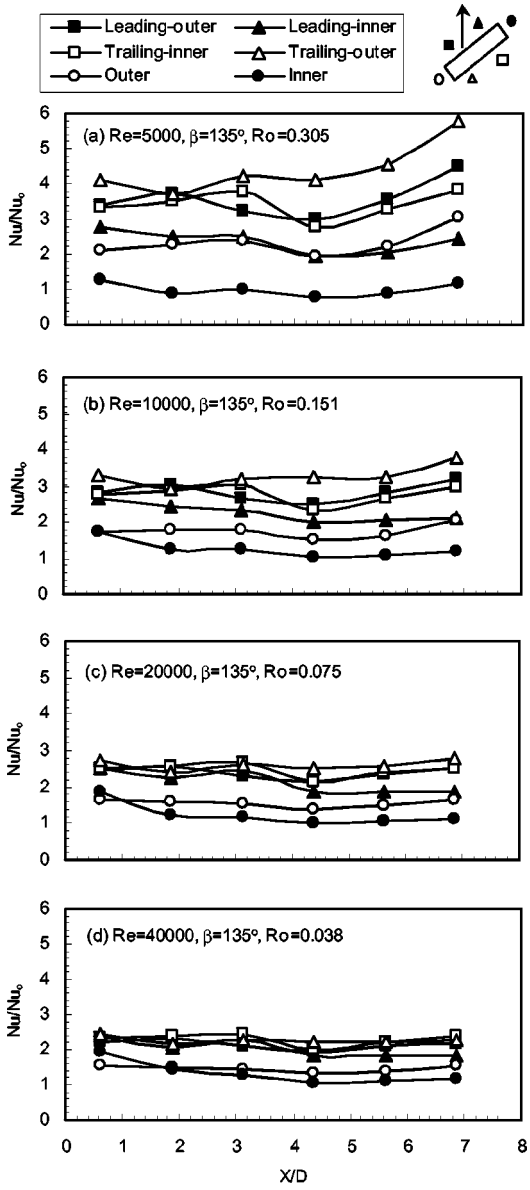

Fig. 11 Nusselt number ratio for rotation dimpled case with β=135 deg

Perhaps this is because the Reynolds number is much closer to the laminar-to-turbulent flow transition region of Re≅2300. Whatever the reason, such a low Reynolds number is not encountered in gas turbines, therefore consideration of this Reynolds number effect is only necessary for those wishing to consider the use of dimples for some other application outside of gas turbine heat transfer.

Figure 10 presents the data for the dimpled channel under rotation, orthogonal to the plane of rotation β=90 deg. It is apparent that there is a definite enhancement due to rotation for the trailing surfaces, which increases with increasing rotation number. Symmetry is achieved relatively well between the two spanwise segments of each dimpled surface, and symmetry between the two side surfaces. Also, the side surfaces experience enhancement equal to the leading surface. This is completely different than the smooth case, where the side surfaces were more equal to the trailing surface.

Figure 11 shows the results for the dimpled channel under rotation, twisted with respect to the plane of rotation (β=135 deg). The trailing-outer surface is enhanced more than the other surfaces, as it benefits from both the shifting of the cold flow toward the outer half of the channel, as well as the local mixing induced by the vortices shed by the dimples. In addition, the trailing-inner and leading-outer surfaces are enhanced (although to a lesser degree) by rotation. This occurs as the Coriolis vortex also serves to distribute some of the cold fluid in the core of the mainstream flow to the other surfaces, allowing the smaller scale dimple induced vortices to capture some of this cold fluid and pull it near to the wall. The outer surface is enhanced more than the inner surface due to the shifting of the majority of the colder flow toward the outer half of the twisted channel under rotation. This behavior was also seen in the smooth duct.

Streamwise Averaged Nusselt Number Ratio. Averaging the streamwise data for each surface provides a method of comparing the surfaces and the effect of rotation. Figures 12 and 13 presents the streamwise averaged data vs. Rotation number for the orthogonal and twisted channel. The solid line plots are for the dimpled channel and the dotted line plots are for the smooth channel.

Figure 12 presents the data for the orthogonal (β=90 deg)

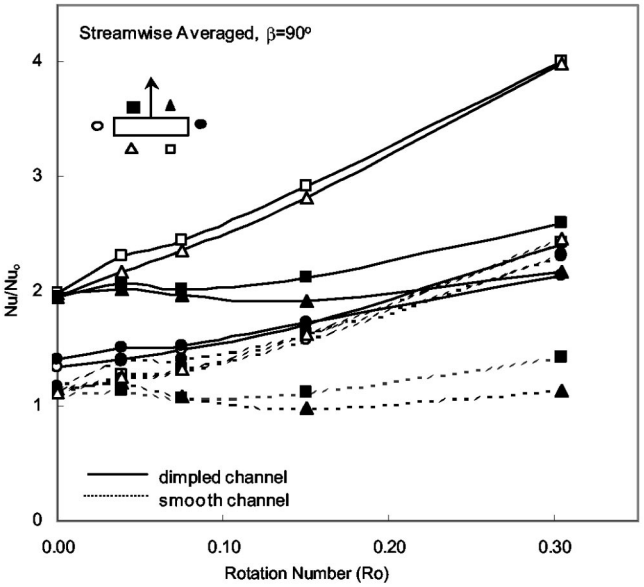

Fig. 12 Streamwise averaged Nusselt number ratio for dimpled and smooth channels with β=90 deg

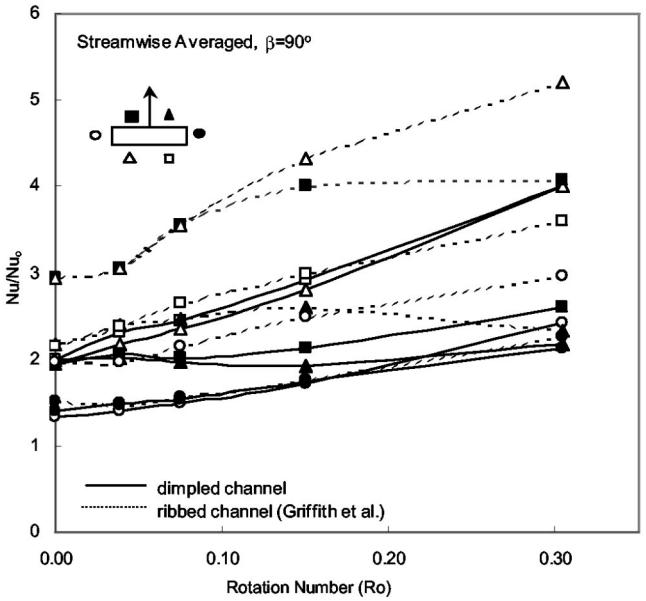

Fig. 14 Streamwise averaged Nusselt number ratio for dimpled and ribbed channels with β=90 deg

dimpled and smooth channel. From this plot, it can be seen that the dimpled trailing surfaces show greater dependence on rotation number than all other surfaces, with nearly 100% improvement in enhancement from the stationary to the highest rotation number case. The dimpled leading surfaces show very little dependence on rotation number due to the stable, thick boundary layer on the leading surface. The slight non-symmetry between the two leading surfaces is due to experimental uncertainty. A most interesting issue arises when comparing the side surfaces (inner and outer) of the dimpled channel to those of the smooth channel. It can be shown that while the side surfaces of the dimpled channel initially experience a higher enhancement without rotation, the smooth channel side surfaces show greater dependence on rotation than the dimpled channel side surfaces. This is possibly attributable to the disruption of the Coriolis vortices by the dimples. For the smooth surface, the Coriolis vortex passes from the center of the channel toward the side surfaces (see Fig. 5), where it enhances the heat transfer from the side surfaces. The secondary flow generated by the dimple has no single principal direction, and likely serves to reduce the intensity of the Coriolis vortices. Because of this, the effect of rotation is reduced for the side walls of the dimpled channel.

Figure 13 shows the streamwise averaged data versus Rotation number for the twisted (β=135 deg) dimpled and smooth channel. The dimpled trailing-outer surface shows the strongest dependence on rotation number and is clearly the primary recipient of enhancement for the twisted channel under rotation. In addition, the dimpled leading-outer and trailing-inner surfaces now show a moderate to high dependence on rotation number. This was also

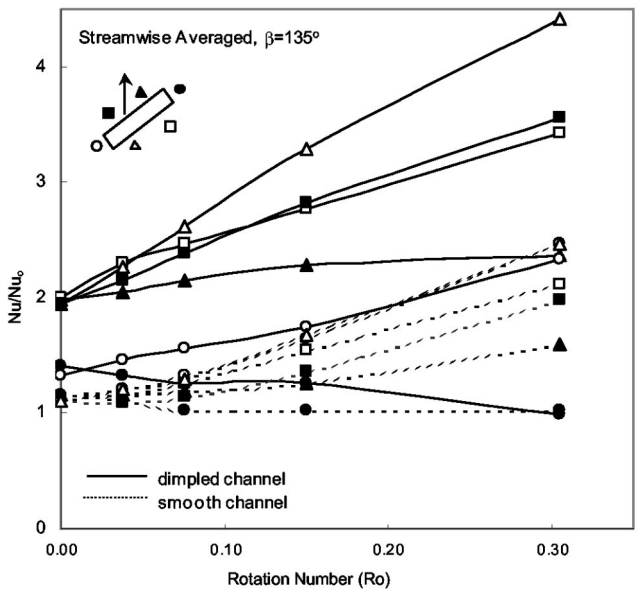

Fig. 13 Streamwise averaged Nusselt number ratio for dimpled and smooth channels with β=135 deg

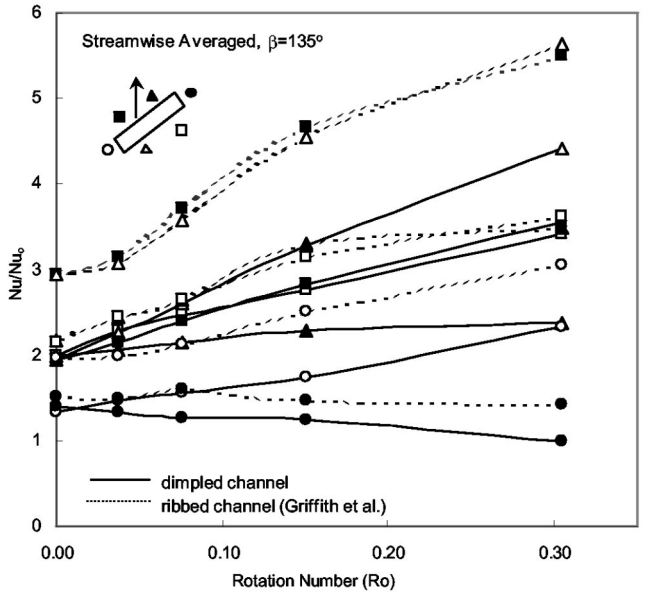

Fig. 15 Streamwise averaged Nusselt number ratio for dimpled and ribbed channels with β=135 deg

explained in the discussion of Fig. 11 where it was noted that the smaller scale vortices shed by the dimple are able to capture some of the lower enthalpy fluid, which is better distributed by the Coriolis vortices for the twisted channel. Again, it is noticed that the side surfaces of the twisted channel are enhanced less by rotation than those of the smooth duct due to the disruption of the Coriolis vortices by the vortices shed by the dimple.

Comparison of Dimpled and Ribbed Channel. Figures 14 and 15 compare the results of this investigation with the ribbed channel investigated by Griffith et al. [9]. We can see that the dimpled channel behaves similarly to the ribbed channel of the same geometrical and flow parameters. While the behavior under rotation is similar, it is noticed that the ribbed channel induces higher heat transfer enhancement when compared to the dimpled channel. This is evident even at the lowest rotation number, indicating that although the dimpled channel provides less enhancement at some surfaces, the behavior is very similar to that of the ribbed channel with increasing rotational effect. Some exceptions include the absence of spanwise variations for the orthogonal (β=90 deg) dimpled channel under rotation. Spanwise variations were quite significant in the case of the ribbed rotating channel due to the 45 deg rib-angle effect. Please note that past research has found that the ribbed channel creates greater pressure drop (friction penalty) than the dimpled channel.

Conclusions

1. Spanwise variations in heat transfer enhancement of the dimpled rotating rectangular channel exist only for the twisted (β=135 deg) orientation.
2. The effect of rotation exhibits similar trends for the dimpled and ribbed surface geometries, however the enhancement of the ribbed channel exceeds the enhancement of the dimpled channel for some surfaces. Both the dimpled and the ribbed channel provide advantageous enhancement compared to the smooth channel.
3. The twisted (β=135 deg) dimpled channel experiences greater overall enhancement than the orthogonal dimpled channel (β=90 deg).
4. For (β=90 deg), enhancement at the trailing surfaces increases by almost 100% from the stationary to highest rotation number case. Also, the leading surfaces show little dependence on rotation number. The side surfaces show slightly less dependence on rotation than those of a smooth duct.
5. For (β=135 deg), enhancement at the trailing-outer surface increases by more than 100% from the stationary to highest rotation number case. In addition, the trailing inner and leading outer surfaces experience nearly identical enhancement, increasing by more than 50% from the stationary to highest rotation number case. The outer surface increases by nearly 100% and the inner surface slightly decreases from the stationary to highest rotation number case.

Acknowledgments

The Advanced Gas Turbine Systems Research (AGTSR) program (project number SR-082) funded this experimental investigation under the supervision of the United States Department of Energy (DOE). The authors greatly appreciate the support of the AGTSR program and the DOE. Dr. H. K. Moon of Solar Turbines, Inc. and Dr. P. Ligrani of the University of Utah provided insight regarding the dimple concept. Without such support, this research would not have been possible.

Nomenclature

AR = aspect ratio
D = hydraulic diameter (m)
D_p = dimple print diameter (m)
L = length of duct (m)
Nu = regionally averaged Nusselt no., hD/k
Nu_o = Nusselt no. in fully developed turbulent nonrotating smooth tube flow
Pr = Prandtl no.
Q = heat transfer (W)
R = mean rotating radius (m)
Re = Reynolds no., $\rho VD/\mu$
R_o = rotation no., $\Omega D/V$
T_{bi} = inlet coolant bulk temperature (K)
T_{bx} = local coolant bulk temperature (K)
T_w = wall temperature (K)
V = bulk velocity in streamwise direction (m/s)
e = rib height (m)
h = heat transfer coefficient ($\mathrm{W/m^2\ K}$)
k = thermal conductivity of coolant (W/mK)
q''_{net} = net heat flux at wall based on projected area ($\mathrm{W/m^2}$)
β = angle of channel orientation
δ = dimple depth
Ω = rotational speed (rad/s)
ρ = density of coolant ($\mathrm{kg/m^3}$)
$\Delta\rho/\rho$ = inlet coolant-to-wall density ratio, $(T_w - T_{bi})/T_w$

References

[1] Schukin, A. V., Koslov, A. P., and Agachev, R. S., 1995, "Study and Application of Hemispherical Cavities for Surface Heat Transfer Augmentation," ASME Paper No. 95-GT-59.
[2] Han, J. C., and Park, J. S., 1988, "Developing Heat Transfer in Rectangular Channel With Rib Turbulators," Int. J. Heat Mass Transf., **31**(1), pp. 183–195.
[3] Wagner, J. H., Johnson, B. V., and Hajek, T. J., 1991, "Heat Transfer in Rotating Passage With Smooth Walls and Radial Outward Flow," ASME J. Turbomach., **113**, pp. 42–51.
[4] Wagner, J. H., Johnson, B. V., and Kooper, F. C., 1991b, "Heat Transfer in Rotating Serpentine Passage With Smooth Walls," ASME J. Turbomach., **113**(3), pp. 321–330.
[5] Parsons, J. A., Han, J. C., and Zhang, Y. M., 1995, "Effects of Model Orientation and Wall Heating Condition on Local Heat Transfer in a Rotating Two-Pass Square Channel With Rib Turbulators," Int. J. Heat Mass Transf., **38**(7), pp. 1151–1159.
[6] Johnson, B. V., Wagner, J. H., Steuber, G. D., and Yeh, F. C., 1994, "Heat Transfer in Rotating Serpentine Passage With Selected Model Orientations for Smooth or Skewed Trip Walls," ASME J. Turbomach., **116**, pp. 738–744.
[7] Dutta, S., and Han, J. C., 1996, "Local Heat Transfer in Rotating Smooth and Ribbed Two-Pass Square Channels with Three Channel Orientations," ASME J. Heat Transfer, **118**, pp. 578–584.
[8] Willett, F. T., and Bergles, A. E., 2000, "Heat Transfer in Rotating Narrow Rectangular Ducts with Heated Sides Oriented at 60deg to the R-Z Plane," ASME Paper No. 2000-GT-224.
[9] Griffith, T. S., Al-Hadhrami, L., and Han, J. C., 2002, "Heat Transfer in Rotating Rectangular Cooling Channels (AR=4) With Angled Ribs," ASME J. Heat Transfer, **124**, pp. 617–625.
[10] Ekkad, S. V., and Han, J. C., 1996, "Effect of Simulated TBC Spallation on Local Heat Transfer Coefficient Distributions Using a Transient Liquid Crystal Image Method," AIAA J. Thermophys. Heat Transfer, **10**(3), pp. 511–516.
[11] Azad, G. M. S., Huang, Y., and Han, J. C., 2000, "Jet Impingement Heat Transfer on Dimpled Surfaces Using a Transient Liquid Crystal Technique," AIAA J. Thermophys. Heat Transfer, **14**(2), pp. 186–193.
[12] Chyu, M. K., Yu, Y., and Ding, H., Downs, J. P., Soechting, O. 1997, "Concavity Enhanced Heat Transfer in an Internal Cooling Passage," ASME Paper No. 97-GT-437.
[13] Moon, H. K., O'Connell, T., Glezer, B., 1999, "Channel Height Effect on Heat Transfer and Friction in a Dimpled Passage," ASME Paper No. 99-GT-163.
[14] Mahmood, G. I., Hill, M. L., Nelson, D. L., Ligrani, P. M., Moon, H.-K., and Glezer, B., 2001, "Local Heat Transfer and Flow Structure on and Above a Dimpled Surface in a Channel," ASME J. Turbomach., **123**, pp. 115–123.
[15] Zhou, F., and Acharya, S., 2001, "Mass/Heat Transfer in Dimpled Two-Pass Coolant Passages with Rotation," Heat Transfer in Gas Turbine Systems, ed., R. J. Goldstein, Ann. N.Y. Acad. Sci., **934**, pp. 424–431.
[16] Han, J. C., Dutta, S., and Ekkad, S. V., 2000. *Gas Turbine Heat Transfer and Cooling Technology*, Taylor and Francis, New York.
[17] Han, J. C., and Dutta, S., 2001, "Recent Developments in Turbine Blade Internal Cooling," Heat Transfer in Gas Turbine Systems, ed., R. J. Goldstein, Ann. N.Y. Acad. Sci., **934**, pp. 162–178.
[18] Incropera, F. P., and DeWitt, D. P., 1996. *Fundamentals of Heat and Mass Transfer*, 4th ed. Wiley, New York.
[19] Kline, S. J., and McClintock, F. A., 1953, "Describing Uncertainties in Single-Sample Experiments," Mech. Eng. (Am. Soc. Mech. Eng.), **75**.

Discussion: "Heat Transfer in Rotating Rectangular Cooling Channels (AR=4) With Dimples" (T. S. Griffith, L. Al. Hadhrami, and J.-C. Han., 2003, ASME J. Turbomach. 125, pp. 555–563)

P. Ligrani
Convective Heat Transfer Laboratory,
Department of Mechanical Engineering,
University of Utah, Salt Lake City, UT 84112-9208

As additional research efforts are conducted, the advantages of using arrays of dimples on the surfaces of internal passages are becoming more apparent. In particular, substantial heat transfer enhancements can be obtained with smaller pressure penalties than provided by other heat transfer augmentation devices, such as rib turbulators. As a result, dimpled surfaces for heat transfer augmentation are encountering wider use in different applications. The purpose of this comment is to point out additional features of the data presented in Fig. 9, which are obtained using a dimpled passage with no rotation.

1 Local and spatially-averaged Nusselt numbers increase as the ratio of dimple depth δ to dimple print diameter D_p increases, provided spherical indentation dimples are used and all other experimental parameters are held constant [20,21]. The δ/D_p ratio of the present study is 0.3. Results from other sources, obtained with no rotation, show that spatially averaged Nusselt number ratios range from 2.53 to 2.6 for $\delta/D_p=0.3$ [21], 2.41 to 2.47 for $\delta/D_p=0.28$ [12], and 2.08 to 2.25 for $\delta/D_p=0.19$ [13]. In each case, and in the present study, similar Reynolds numbers are used, and the ratio of channel height to dimple print diameter is 1 to 2. The spacing and arrangement of dimples on the test surface are the same in the present study as used by Burgess et al. [21], and very similar to the dimple spacings and arrangements used by Chyu et al. [12], and Moon et al. [13]. As the authors point out, spatially averaged Nusselt number data, presented as a ratio, are nearly independent of Reynolds number. Nusselt number ratio variations are also quite small at given Reynolds number as the ratio of channel height to dimple print diameter changes from 0.37 to 1.49 [13].

2 Nusselt number ratios, presented in Fig. 9, for no rotation, are about 2.0 for three of the Reynolds numbers investigated. This is lower than the expected value of 2.53–2.6 for the same δ/D_p. This appears to be tied to the limitations imposed by the rotating test rig, and the use of only one thermocouple to measure the "regionally averaged" surface temperature at one point on a surface segment with multiple dimples (Fig. 3). Large surface Nusselt number variations are present on dimpled surfaces in channels [12,13,20,21]. Accurate spatially averaged Nusselt numbers can only be obtained from spatially-averages of locally measured values over an area comprised of at least one complete period of dimple surface geometry [12,13,14,21].

3 The authors are congratulated for conducting difficult experiments in stationary and rotating environments where accurate heat transfer data are difficult to obtain.

References

[20] Gortyshov, Y. F., Popov, I. A., Amirkhanov, R. D., and Gulitsky, K. E., 1998, "Studies of Hydrodynamics and Heat Exchange in Channels with Various Types of Intensifiers," Heat Transfer, Proc., 11th IHTC, Vol. 6, pp. 83–88.

[21] Burgess, N. K., Oliveira, M. M., and Ligrani, P. M., 2003, "Nusselt Number Behavior on Deep Dimpled Surfaces Within a Channel," ASME J. Heat Transfer, **125**(1) pp. 11–18.

Closure to Discussion of "Heat Transfer in Rotating Rectangular Cooling Channels (AR=4) With Dimples" (2003, ASME J. Turbomach., 125, p. 564)

The authors appreciate Dr. Ligrani's comment on the paper. The discrepancy of heat transfer enhancement on the dimpled surface reported by different investigators might be due to the use of different measurement technique for the data taken and reduction. In addition to the aforementioned studies, for example, Zhou and Acharya [15] reported that the heat transfer enhancements of the dimpled surface for nonrotation could be about 1.5–2 times the smooth channel values for a dimple depth to print diameter ratio of 0.29 by using the naphthalene sublimation mass-transfer technique. Moon and Lau [22] showed that the dimpled surface heat transfer for nonrotation enhanced about 1.6–1.8 times the smooth-channel values for the dimple depth to print diameter ratios around 0.2–0.23 by using the standard aluminum plate with heaters and thermocouples. These heat transfer enhancement ratios are close to the present study's values for nonrotation by using the standard copper plate with heaters and thermocouples. But they are lower than the aforementioned values reported by Chyu et al. [12] using the transient liquid crystal technique, Moon et al. [13] using the transient liquid crystal technique, and Burgess et al. [21] using the IR camera technique. It is likely that using different measurement technique and data analysis could produce 10–20% different heat transfer enhancement values for turbulent channel flow through such a complex dimpled surface.

The present study used the traditional copper plate with heaters and thermocouples technique. The purpose was to obtain the regionally averaged heat transfer coefficient per copper plate. According to Fig. 3 in the paper, each copper plate is 2.54 cm by 2.54 cm facing to the cooling flow and with 0.3175-cm thickness. The estimated maximum Biot number of the copper plate is around 0.0022 for the highest heat transfer coefficient case at Re=40,000 of the present study. This means that the temperature gradient within the copper plate is small as expected by using this kind of standard measurement technique. On the other hand, in order to produce 20% heat-transfer coefficient's discrepancy in the copper plate, it requires 7°C of temperature gradient within each copper plate. This unlikely would happen in the present test condition ($Tw=67$°C, $Tb=32$°C). In addition, the high-conductivity copper plate with dimples represents the true span-averaged heat transfer coefficient including the potential end-wall effect from the channel smooth-side walls. For example, the potential smooth-side wall effect on the span-averaged heat transfer coefficient could not be included by viewing only the central 5-dimple area using the IR camera technique shown in Fig. 2 by Mahmood et al. [14]. The central 5-dimple area only might potentially produce higher heat transfer enhancement than the truly span-averaged values including the potential smooth end-wall effect.

To solve the issue, the authors plan to further investigate this topic. Again, the authors do appreciate Dr. Ligrani's insightful comment on the important dimple cooling technology for turbine blade cooling designs.

References

[22] Moon, S. W., and Lau, S. C., 2002, "Turbulent Heat Transfer Measurements on a Wall with Concave and Cylindrical Dimples in a Square Channel," ASME TURBO EXPO 2002, GT-2002-30208.

